

# Improved current transport properties of post annealed Y1Ba2Cu3O7-x thin films using Ag doping

**Clausen, Thomas; Skov, Johannes; Jacobsen, Claus Schelde; Bukh, K R; Bollinger, Mikkel; Tobiasen, B. P.; Sager, M. P.; Chorkendorff, Ib; Larsen, J**

*Published in:*
Journal of Applied Physics

*Link to article, DOI:*
10.1063/1.361473

*Publication date:*
1996

*Document Version*
Publisher's PDF, also known as Version of record

# Improved current transport properties of post annealed $Y_1Ba_2Cu_3O_{7-x}$ thin films using Ag doping

T. Clausen, J. L. Skov, C. S. Jacobsen, K. R. Bukh, M. V. Bollinger, B. P. Tobiasen, and M. P. Sager
*Physics Department, Technical University of Denmark, Bldg. 309, DK-2800 Lyngby, Denmark*

I. Chorkendorff and J. Larsen
*Physics Department, Technical University of Denmark, Bldg. 307, DK-2800 Lyngby, Denmark*

(Received 31 July 1995; accepted for publication 2 January 1996)

The influence of Ag doping on the transport properties of $Y_1Ba_2Cu_3O_{7-x}$ thin films prepared by Y, $BaF_2$, and Cu co-evaporation and optimized *ex situ* post annealing has been investigated. Both undoped and Ag doped films have values of $T_c$ above 90 K, but $J_c$ (77 K) is highly dependent on the nominal thickness ($t_{nom}$) of the as-deposited film. For undoped films with $t_{nom} \leqslant 300$ nm $J_c$ (77 K) ($\geqslant 10^6$ A/cm$^2$) decreases monotonically with increasing film thickness. Above 300 nm $J_c$ (77 K) decreases rapidly to values below $5\times10^5$ A/cm$^2$. Ag doped films with $t_{nom} \geqslant 200$ nm have higher $J_c$ (77 K) values than those of undoped films. Ag doped films have a maximum in $J_c$ (77 K) around 250 nm. As for the undoped films, there is a large decrease in $J_c$ (77 K) for Ag doped films with $t_{nom} \geqslant 300$ nm. It was found that the higher values of $J_c$ (77 K) for the Ag doped films were due to a better epitaxial growth of the YBCO compound. The low values of $J_c$ (77 K) for both undoped and Ag doped single layer films with $t_{nom} \geqslant 300$ nm were found to be due to the absence of 1–2–4 inclusions in these films. Based on these findings high $J_c$ (77 K) films with $t_{nom} > 300$ nm were grown by successive deposition and annealing of films with $t_{nom} < 300$ nm on top of each other. A $2\times150$ nm undoped film was found to have a $J_c$ (77 K) value of 4, $1\times10^6$ A/cm$^2$. This is almost a doubling of the $J_c$ (77 K) value as compared to the value for the 300 nm single layer undoped film ($2{,}2\times10^6$ A/cm$^2$). Ag doped double layer films of $2\times150$ nm and $2\times215$ nm had comparable $J_c$ (77 K) values ($5{,}8\times10^6$ and $5{,}6\times10^6$ A/cm$^2$, respectively). In comparison with the undoped $2\times150$ nm film $J_c$ (77 K) is thus further increased (by about 50%) when doping with Ag. © *1996 American Institute of Physics.* [S0021-8979(96)03208-2]

## I. INTRODUCTION

High-$T_c$ superconducting $Y_1Ba_2Cu_3O_{7-x}$(YBCO) thin films can be grown by several techniques. The $BaF_2$ co-evaporation technique has proven superior in combination with optimized *ex situ* post annealing at low oxygen partial pressures.[1–7] In general, films processed under these conditions have a good surface morphology with no large surface outgrowths, high transition temperatures ($T_c$), high values of the critical current density ($J_c$) and good microwave properties.[3–7] These good properties can be obtained only if the YBCO thin films are grown on special substrates. Good lattice matching in the $a-b$ plane is necessary to reduce film strain and encourage 1–2–3 YBCO $c$-axis growth. Furthermore, it is important for the substrate to be able to withstand the high processing temperatures (750–900 °C) and the annealing environment in order to reduce interdiffusion between the YBCO and the substrate elements. It has been shown that $LaAlO_3$ satisfies these requirements for the $BaF_2$ co-evaporation process, with *ex situ* post annealing incorporating a wet oxidation step.[5,8] On the other hand, we have found that MgO substrates degrade in the wet environment leading to Mg diffusion into the growing YBCO film, and as a result of that the superconducting properties degrade ($T_c \approx 82-84$ K).[9]

Doping of YBCO have been studied intensively ever since the discovery of the high $T_c$ 1–2–3 YBCO compound.[10–25] For instance, by doping YBCO with Ag or Au both $T_c$ and $J_c$ can be enhanced depending on the growth parameters. The incorporation of Ag into YBCO has been postulated to give several effects; (i) improved values of $J_c$ due to intergranular diffusion of Ag resulting in reduced contact resistance between the superconducting grains,[11,15,17,19] (ii) a larger amount of the YBCO film is $c$-axis oriented[13,21] also resulting in improved values of $J_c$ and (iii) if the annealing temperature exceeds the melting point of the Ag/YBCO-phase, the Ag atoms can diffuse into the YBCO lattice and substitute Cu atoms at the Cu(1) sites. The Ag atom thereby bonds to an additional electron, thus increasing the hole concentration resulting in an increased $T_c$.[22]

Recently Pinto *et al.*[13] have demonstrated improved microwave performance of Ag doped pulsed laser deposition (PLD) YBCO thin film (thickness; 200 nm) microbridge resonators. They found that grain boundary weak links in undoped YBCO films are the main reason for large values of the surface resistance ($R_s$) and its dependence on the microwave input power levels.[13] They ascribed the better microwave performance of the Ag doped films to a better epitaxy of the films in accordance with other reports on the subject.[13,19–21] In this paper, we study the effect of Ag doping of YBCO thin films grown using the $BaF_2$ coevaporation process and *ex situ* post annealing.

It is a general observation that $J_c$ decreases somewhat with increasing film thickness for *ex situ* post annealed YBCO films.[6,7,23,26] This behavior has been explained by a

 0021-8979/96/79(9)/7062/7/$10.00 

TABLE I. Results on stoichiometric check on 500 nm thick Ag doped YBCO film with ICP and EDAX.

| Element | Stoichiometric compound (at. %) | ICP Ag–YBCO (at. %) | ICP bulk-YBCO (at. %) | EDAX Ag–YBCO (at. %) |
|---|---|---|---|---|
| Y | 7.69 | 7.31 | 7.84 | 7.49 |
| Ba | 15.38 | 15.53 | 15.07 | 15.41 |
| Cu | 23.08 | 23.31 | 23.23 | 23.24 |
| O | 53.85 | NA[a] | NA[a] | NA[a] |

[a]NA means that the information is not available from the technique used. For the calculation we have assumed that the oxygen content $x$ is close to 7.

decreasing density of 1–2–4 stacking faults with increasing film thickness assuming that the stacking faults act as core type flux pinning centers.[26] In this paper, we show that the 1–2–4 phases more likely make an additional contribution to $J_c$ below 80 K and we report on a novel technique that circumvents the problem on decreasing $J_c$ with increasing film thickness. The novel technique employs a fabrication of YBCO films in sequential steps, i.e., make multiple film deposition and annealing steps.

## II. EXPERIMENT

The thin films [150 nm $\leqslant t_{\mathrm{nom}}$ (nominal film thickness)$\leqslant$500 nm] were deposited by co-evaporation of Y (99,9%) and Cu (99,999%) from electron guns and $BaF_2$ (99,9%) from an effusion cell onto polished $8\times8$ mm$^2$ and $10\times10$ mm$^2$ (100) $LaAlO_3$ substrates in a Vacuum Generators UHV chamber with a base pressure of less than $10^{-9}$ Torr. During deposition the chamber pressure increased to about $5\times10^{-7}$ Torr. The substrates were rotated at 10 rpm and were held close to room temperature (27 °C) during deposition. The stoichiometry of the as-deposited films were controlled by monitoring the evaporation rates and checked for each deposition using the inductive coupled plasma (ICP) technique and energy dispersive x-ray analysis (EDAX). In Table I are shown a typical result of a stoichiometric check with ICP and EDAX for a bulk YBCO piece compared with a 500 nm Y–$BaF_2$–Cu thin film coated with Ag. Within a few percent, the film has the right stoichiometric ratio (Table I).

*Ex situ* post annealing was performed in a quartz tube furnace (with quartz getters) using a two-step annealing technique consisting of a high temperature step followed by a lower temperature step. The first step was a one hour annealing at a temperature of 800 °C in a Ar–$O_2$ mixture flow of 1000 sccm. The oxygen partial pressure, $p(O_2)$, was 100 Pa and the gas was bubbled through deionized $H_2O$ starting at 775 °C during ramp up (20 °C/min) and ending also at 775 °C during ramp down (5 °C min). The second step was a one hour annealing at 525 °C in 1 atm dry oxygen with a flow rate of 200 sccm. Switching from the low-$p(O_2)$ to the high $p(O_2)$ regime was done at 550 °C during ramp down. The Ag doping (5 wt %) was achieved by coating the amorphous $Y_1(BaF_2)_2Cu_3$ film with Ag (99,999%) overlayers prior to the *ex situ* post annealing.

The superconducting properties of the annealed films were evaluated by measuring the zero resistance transition temperature ($T_c$) and the critical current density ($J_c$) for temperatures ranging from 50 K to 88 K. The surface morphology was examined by scanning electron microscopy (SEM) and atomic force microscopy (AFM). The degree of the intergranular diffusion of Ag into the YBCO lattice and the crystalline quality of the YBCO film were studied with Auger electron spectroscopy (AES) and x-ray diffraction (XRD), respectively.

The measurement of $T_c$ was done by measuring the dependence of film resistivity on temperature (77–300 K) by a standard four-point probe technique using a lock-in-amplifier (PAR Model 186 SYNCHRO-HET). Indium bits were pressed in contact with the film in order to minimize the contact resistance between the probes and the superconductor. Typical current levels were around 10 $\mu$A. The $a-b$ plane $J_c(T)$ was determined from ac-magnetization experiments. The sample was mounted close to one of two balanced pick-up coils (diameter 5 mm) which were suspended in a 6 Hz ac magnetic field. The signal $S(t)$ from the pick-up coils was recorded, time integrated and plotted against the excitation signal $A(t)$, thereby obtaining magnetization hysteresis loops. $J_c$ was evaluated from the height of the magnetization loops (self-field conditions). In general, this gives a value of $J_c$ which is somewhat lower than what is measured using a current-voltage ($I$–$V$) characterization method, because no voltage criterion is set in the magnetization experiments.

Scanning electron microscopy for near-surface imaging of the YBCO films was performed using a 30 keV primary electron beam from a Phillips XL20 instrument equipped with an energy dispersive x-ray analysis facility. Atomic force microscopy was performed using a constant force method on an AFM Rasterscope™ 4000 DME instrument.

Phase identification was done with x-ray diffraction using a Phillips PW 1710 $\Theta$-$2\Theta$ diffractometer with diverging slits. The sample holder for the x-ray diffractometer was made from polystyrene with a recess for placing the samples. The samples were mounted with wax and aligned with respect to the $CuK_\alpha$ beam by pressing the samples gently in place with another polystyrene plate face to face with the sample holder. $2\Theta$ was scanned from 10° to 90° with a scan rate of 0.6°/min. A PHI 590 A scanning Auger microprobe (SAM) with a base pressure of less than $2\times10^{-10}$ Torr, combined with *in situ* argon ion milling, was used to study the compositional properties of the YBCO/Ag films. The Auger spectra were obtained with a 10 keV primary beam corresponding to a beam spotsize of a few microns. The $Ar^+$ sputtering ion energy was 2 keV and the fluency was 25 mA cm$^{-2}$. During the various sputtering cycles the operating pressure was increased from about $2\times10^{-10}$ to $2\times10^{-7}$ Torr by leaking argon gas into the working chamber. Atomic concentration profiles were obtained from the Auger spectra by using standard table sensitivity factors for all the involved atomic elements at the chosen energy of the primary beam.

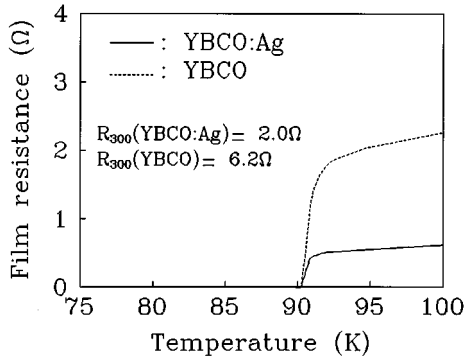


FIG. 1. Film resistance vs temperature for undoped 300 nm film (dashed line) and Ag doped 300 nm film (solid line).

## III. RESULTS

For the undoped films we found that $T_c$>90 K with a transition width $\Delta T_c$<1 K (Fig. 1). The best films had $T_c$'s just below 92 K ($t_{\text{nom}}$>300 nm). The ratio between the film resistance at 300 K and the film resistance at 100 K was below 3 (2.7–2.9) for the undoped films. $J_c$ (77 K) was found to decrease with increasing nominal film thickness with $J_c$ (77 K) values ranging from $2.0\times10^5$ A/cm$^2$ to $4.5\times10^6$ A/cm$^2$ (Fig. 2). As can be seen from Fig. 2, there is a large decrease in $J_c$ (77 K) for films with $t_{\text{nom}}$>300 nm. For a 1 $\mu$m wide microbridge this means that the maximum critical current is about 7 mA (77 K) for films with $t_{\text{nom}}\leqslant$300 nm, while for films with $t_{\text{nom}}$>300 nm, the maximum critical current that can be carried is only about 1 mA (77 K). McIntyre *et al.*[26] have found, for *ex situ* post annealed chemically derived films, that a maximum critical current of about 5 mA can be applied to a microbridge of 1 $\mu$m width irrespective of the film thickness (<500 nm). Thus, the growth mode for our films seems to change when the film thickness exceeds 300 nm. This change in growth mode can probably be shifted to a larger thickness if the annealing conditions are further optimized as it has been reported by Hou *et al.*[7] However, high values of $J_c$ (77 K) ($\geqslant10^6$ A/cm$^2$) are not expected for undoped films with $t_{\text{nom}}\geqslant$400 nm even when the annealing conditions are further optimized.[7]

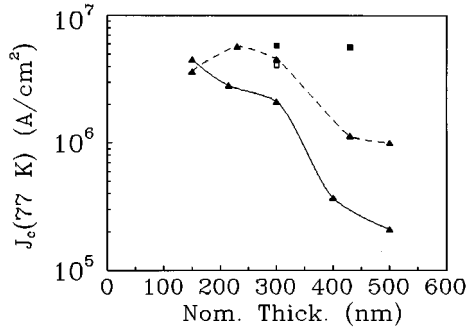


FIG. 2. Critical current density measured at 77 K, $J_c$ (77 K), vs the nominal film thickness for undoped films (solid line), Ag doped films (dashed line), undoped double layer film (open square), and Ag doped double layer films (filled squares). Lines are guides for the eye.

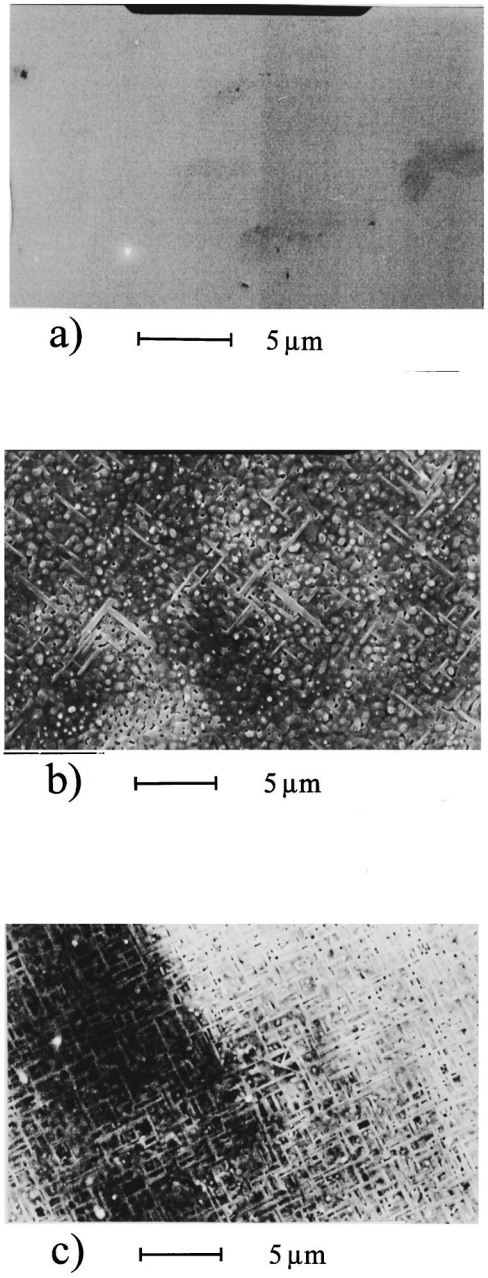


FIG. 3. SEM pictures of surface morphology of undoped films with different film thicknesses, (a) 150 nm, (b) 300 nm, and (c) 500 nm.

SEM pictures of the surface morphology of the undoped films are shown in Fig. 3. 150 nm films are smooth with no visible surface structures [Fig. 3(a)] When the film thickness is increased $a-b$ axis surface structures become visible [Fig. 3(b)] and for films with $t_{\text{nom}}$>300 nm the $a-b$ surface structures cover all of the surface [Fig. 3(c)] Hou *et al.*[7] have found a similar surface morphology behavior when comparing *ex situ* post annealed films of different thicknesses. They also found that $J_c$ decreases with increasing film thickness.[7]

For the Ag doped films, we also found that $T_c$>90 K with $\Delta T_c$<1 K (Fig. 1). These films showed good metallicity with a ratio between the film resistance at 300 K and the film resistance at 100 K being close to 3. Again, the best films had $T_c$'s just below 92 K ($t_{\text{nom}}$>300 nm). For Ag doped

films with $t_{nom}>150$ nm $J_c$ (77 K) was significantly improved in comparison with undoped single layer films, but for the 150 nm Ag doped film $J_c$ (77 K) was lower than what could be obtained for an undoped film (Fig. 2). As can be seen from Fig. 2, $J_c$ (77 K) has a maximum around a 250 nm Ag doped film ($5.7\times10^6$ A/cm$^2$). For the microbridge device described previously this means that a maximum critical current of 14 mA (77 K) can be carried for Ag doped films with thicknesses between 250–300 nm. This is a doubling of the current carrying capacities in comparison with the capacities for undoped films. As was the case for the undoped films, the growth mode also seems to change with increasing thickness for the Ag doped films as seen by the low values of $J_c$ (77 K) for Ag doped films with $t_{nom}>300$ nm (Fig. 2). If optimized with respect to the annealing conditions, we believe that values of $J_c$ (77 K) well above $10^6$ A/cm$^2$ can be achieved for 400–500 nm Ag doped films, but the current carrying capacities for a device will probably remain close to that of the 200–300 nm Ag doped films.

SEM and AFM pictures of the surface morphology of the Ag doped films are shown in Fig. 4 and Fig. 5, respectively. As can be seen, droplets have nucleated on the surface of an otherwise hard and smooth film. From EDAX measurements, it was found that the droplets consisted mostly of Ag with less than 1 at % Ag in the underlying YBCO matrix. From AFM (Fig. 5), it was found that the height of a large number of the droplets exceeded the nominal YBCO film thickness. The droplets were only loosely bound to the YBCO film and were easily removed with for instance a pair of tweezers or a light rinse/etch [Fig. 4(c)]. From AES experiments (Fig. 6), it was found that the Ag droplets extend into the YBCO film [Fig. 6(a)], while outside the droplet region the film was quite homogeneous with little Ag in the YBCO matrix [Fig. 6(b)]. Note that the right stoichiometric ratio between Y, Ba, and Cu (1:2:3) can not be obtained from Fig. 6(b). This is in contrast to the findings in Table I, where we find the right stoichiometric ratio using ICP and EDAX. The discrepancy is due to the sensitivity factors used for the calculation of the atomic concentrations in the AES plots (Fig. 6), and has recently been corrected by Selvam.[26]

XRD experiments on undoped and Ag doped 500 nm films (Fig. 7) showed that both were preferentially $c$-axis oriented with a somewhat higher yield (30%) from the $(00l)$ planes for the Ag doped film. When calculating the $c$-axis length on the basis of the position of the $(00l)$ reflections, it was found that $c_{undoped}=11.70$ Å and $c_{Ag\text{-}doped}=11.68$ Å. The expanded $c$-axis length for the undoped 500 nm film indicates that the epitaxy is better (larger grain size/smaller grain boundary angle/stress relaxation) for the Ag doped 500 nm film. Alternatively, the difference in the $c$-axis length for the two films can be explained by a different oxygen content in the YBCO phase. In any case, they can both explain the difference in $J_c$ (77 K) between the undoped and Ag doped films. We will return to this point in the next section where we discuss the results in more detail.

In addition to the YBCO $(00l)$ diffraction peaks several impurity peaks were found (Fig. 7). The main impurity peaks were identified as 1–2–4 $(h00)$ and $(hh0)$ diffraction peaks, but also small amounts of 2–1–1 phases were detected from XRD (Fig. 7). These impurity phases with their corresponding orientational behavior have been observed by other authors studying post annealed YBCO films.[27–29] The influence of these impurity phases on the current transport properties will also be discussed in more detail in the next section.

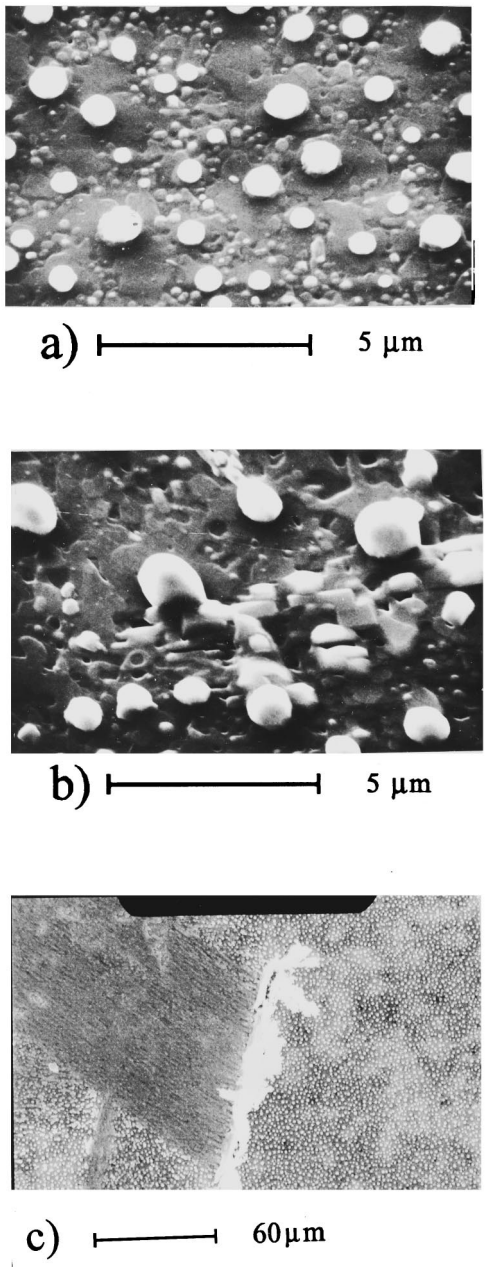


FIG. 4. SEM pictures of surface morphology of Ag doped films, (a) 250 nm, (b) 430 nm, and (c) Ag droplets have been removed with a pair of tweezers. Note the different length scales.

## IV. DISCUSSION

Transport properties of post annealed YBCO thin films are sensitive to the thickness of the as-deposited films and the annealing parameters. This is clear from our results presented above and the results of several other groups.[1–7,27–29] McIntyre *et al.* have reported on the $J_c$ dependence of film thickness for similar post annealed films.[27] They showed that there is a correlation between the density of 1–2–4 stacking

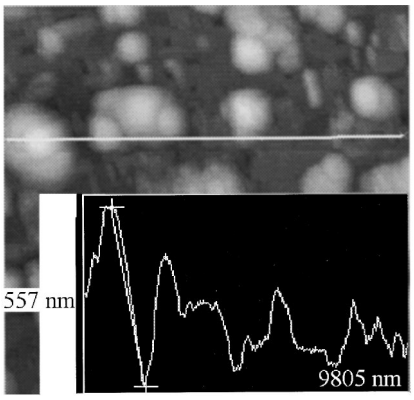


FIG. 5. AFM picture of surface morphology of Ag doped film. The inset shows a line surface roughness scan across the surface (white line on the AFM picture).

faults and $J_c$ in that the 1–2–4 stacking faults act as planar core type flux pinning centers thereby increasing $J_c$. They also found that the density of stacking faults decreases with increasing film thickness for post annealed films because of a change in the growth mode.[27] This is in accordance with Clemens *et al.* who have found that the 1–2–4 preferentially nucleates at the substrate/film interface.[29] Thus, $J_c$ is expectedly higher for thinner post annealed films. We have studied the dependence of $J_c$ in the temperature range from 50–88 K for different samples (Fig. 8). The samples represent two types of growth; namely (i) a film with a thickness below 300 nm (this film is expected to have a large number of 1–2–4 inclusions) and (ii) a film with a thickness above 300 nm (this film is expected to consist primarily of the 1–2–3 phase with only a small density of 1–2–4 inclusions). From Fig. 8, it is seen that there is a kink in the curve at $T \approx 79$ K for the two films that are expected to contain a large density of 1–2–4 inclusions. This indeed indicates the presence of 1–2–4 phases in these films since this phase becomes superconducting around 80 K. The $J_c - T$ curve for the single layer 430 nm film is smooth and that film is therefore believed to have only a small density of 1–2–4 inclusions that can contribute to the total value of $J_c$. The results presented in Fig. 8 thus explains the low values of $J_c$ for films with a thickness above 300 nm for Ag doped and undoped films (Fig. 2). For films with a thickness below 300 nm, $J_c$ has contributions both from the 1–2–3 phase ($<T_c$) and the 1–2–4 phase ($<80$ K).

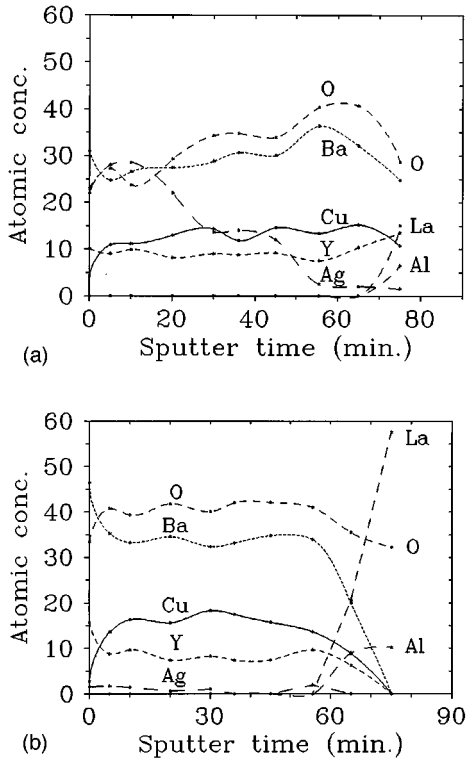


FIG. 6. AES sputter depth profiles of an Ag doped film (a) on a droplet and (b) between the droplets. Standard sensitivity factors were used to calculate the atomic concentrations.

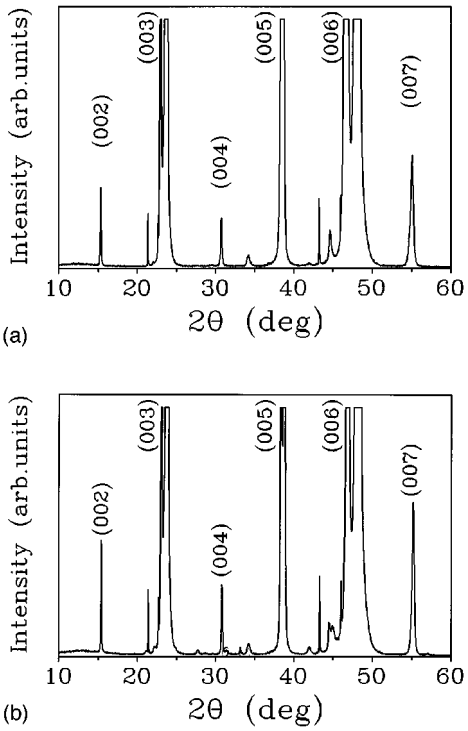


FIG. 7. XRD $\theta$–$2\theta$ scans of YBCO films, (a) undoped 500 nm film and (b) Ag doped 500 nm film.

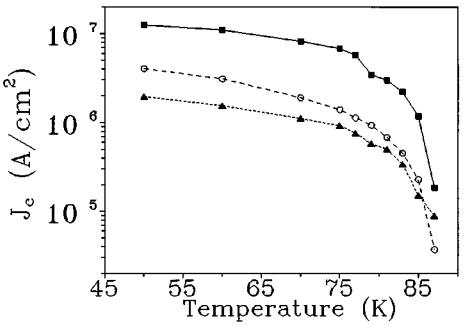


FIG. 8. Critical current density, $J_c$ vs temperature for Ag doped films; solid line: 250 nm film, long dashed line: 430 nm film and short dashed line: 300 nm+430 nm double layer film.

Optimum annealing conditions for post annealed YBCO thin films have been reported by Siegal *et al.*[5] and Hou *et al.*[7] They find that there are two optimum lines in the $p(O_2)$-$T$ diagram depending on the desired property of the YBCO thin film. If a good crystalline film is wanted in preference to a film with a high value of $J_c$, a higher annealing temperature is required for a given oxygen partial pressure.[5,7] As described in the experimental section, our films are annealed in an oxygen partial pressure of 100 Pa at 800 °C. This means, in terms of the results of Siegal *et al.*[5] and Hou *et al.*,[7] that we are 25 °C below the optimum temperature for good crystalline films, but 50 °C above the optimum temperature for high $J_c$ films. However, we are annealing in the optimum processing window for $BaF_2$ post annealed films as defined by Hou *et al.*[7] Moreover, we are annealing for one hour while both Siegal *et al.*[5] and Hou *et al.*[7] annealed their films for only 30 min. The difference in annealing time may change the position of the two optimum lines since the annealing time is a very important parameter in obtaining good quality films.

The 1–2–4 phase can be stabilized by the use of lower temperatures for a given oxygen partial pressure,[30] but for the temperature and the oxygen partial pressure that we use the 1–2–3 phase is the only stable phase.[30] Still, 1–2–4 inclusions are found that have distinct normal-superconducting properties (Figs. 2, 7, and 8). The optimum line for high values of $J_c$ is shifted towards lower temperatures for a given oxygen partial pressure at the cost of a deteriorated crystal quality.[5,7] We believe that this optimum is governed by the creation of 1–2–4 inclusions in the 1–2–3 crystal. Beyond the optimum line for high values of $J_c$ (i.e., lower temperatures) more 1–2–4 inclusions form that significantly reduces both $T_c$ and $J_c$, $T_c$ decreases to a lower value in the presence of 1–2–4 inclusions. $T_c$ changes from just over 90 K for 150–300 nm films (with 1–2–4 inclusions) to values well above 91 K for films with a thickness above 400 nm (with little or no 1–2–4 inclusions).

Ag doped films in general show a significant improvement in $J_c$(77 K) in comparison with undoped films. Above a thickness of 250 nm the Ag doped and undoped films have a similar dependence on the thickness of the as-deposited film. From SEM, AFM, and AES analyses it was shown that Ag nucleates in droplets which are dispersed across the film. The droplets extend into the YBCO film and the total thickness of the droplets exceeds that of the YBCO film. The droplets can thus be thought as effective vertical pinning centers that pin flux vortices along their length when a current is passed through the film. XRD showed that the epitaxy of the YBCO film did benefit from Ag doping. This suggests that the improved transport properties for Ag doped films with a thickness above 200 nm is not entirely due to pinning effects but also due to an improved growth of YBCO. Although it is difficult to conclude from our experiments which mechanism is most responsible for the improved behavior, the formation of smaller-angle junctions, larger grain sizes, and relaxation of residual stresses in the YBCO film caused by Ag are the most probable mechanisms. The 150 nm film did not benefit from Ag doping. On the contrary the Ag doped 150 nm film had worse transport properties than did the undoped 150 nm. This could be due to thickness variations in the as-deposited very thin Ag layer for the 150 nm films or the very thin Ag layer may not have been continuous.

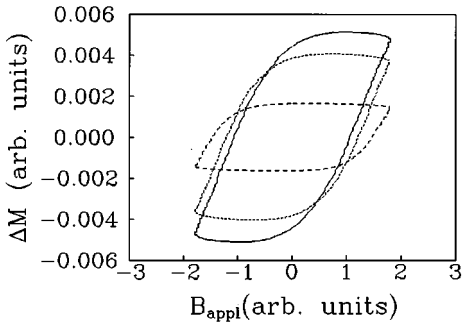


FIG. 9. Magnetization curves for 150 nm undoped films with different annealing parameters; solid line: 800 °C/60 min+525 °C/60 min, short dashed line: 800 °C/15 min+525 °C/60 min, long dashed line: 800 °C/15 min +525 °C/15 min.

Based on the results from the single layer films (Figs. 1–8), there is a possibility that $J_c$ can be further increased for films with $t_{nom}>300$ nm by growing a YBCO multilayer film. The multilayer film should thus consist of several layers with a thickness ranging from 150 to 300 nm and after each deposition the film should be annealed. The previously used annealing profile can not be used directly because of the total thermal budget. We have studied the effects on $J_c$ (77 K) by changing the time at the two annealing steps on undoped single layer films with a thickness of 150 nm. The results (Fig. 9 and Table II) show that a decrease in time of the high annealing step at 800 °C does not seriously affect the value of $J_c$(77 K). However, if the time at the low annealing step at 525 °C is decreased the value of $J_c$(77 K) is significantly reduced (Fig. 9 and Table II). Therefore, an annealing profile with 15 min at 800 °C and 60 min at 525 °C was chosen in order to reduce the total thermal budget for the multilayer film.

A double layer film ($t_{nom}=2\times150$ nm) was grown with the deposition/annealing technique discussed above. The film was found to have a value of $J_c$(77 K) of $4.1\times10^6$ A/cm$^2$ (Fig. 2). This value is almost twice the value of $J_c$(77 K) for a 300 nm single layer film [$J_c$(77 K)$=2.2\times10^6$ A/cm$^2$ (Fig. 2)]. Compared to a Ag doped single layer film with a thickness of 300 nm [$J_c$(77 K)$=4.5\times10^6$ A/cm$^2$ (Fig. 2)], we find that the $J_c$ values are almost the same. This implies that a further enhancement of $J_c$ can be achieved by doping the multilayer film with Ag. The SEM and AFM pictures (Figs.

TABLE II. Effect on $J_c$ (77 K) by changing the annealing time at both the annealing step (800 °C) and the oxygenation step (525 °C).

| Annealing parameters (°C)/(min) | Film thickness (nm) | $T_c$ (K) | $J_c$ (77 K) A/cm$^2$ |
|---|---|---|---|
| 800/60+525/60 | 150 | 89.6 | $4.5\times10^6$ |
| 800/15+525/60 | 150 | 89.9 | $3.5\times10^6$ |
| 800/15+525/15 | 150 | 89.1 | $1.4\times10^6$ |

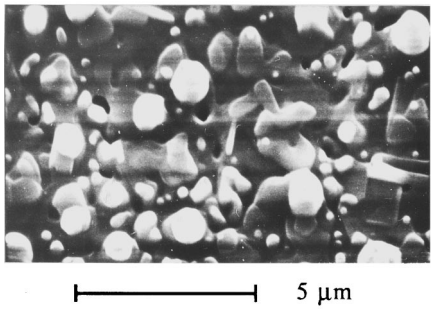


FIG. 10. SEM pictures of surface morphology of Ag doped 300 nm+430 nm double layer film.

4 and 5) of the annealed Ag doped single layer films showed that the Ag nucleates in droplets on the surface of the YBCO. The Ag doped double layer film can thus be grown by (i) depositing a $Y_1(BaF_2)_2Cu_3$ film on the $LaAlO_3$ substrate; (ii) covering the film with Ag (iii) annealing using the double layer annealing procedure; (iv) depositing a new $Y_1(BaF_2)_2Cu_3$ film; and (v) annealing using the double layer annealing procedure. The Ag droplets on top of the first YBCO layer are used as dopant material in the second YBCO layer matrix. With $t_{nom}=2\times150$ nm YBCO and Ag deposited between the layers, a $J_c$(77 K) value of $5.8\times10^5$ A/cm$^2$ was achieved (Fig. 2). $J_c$ is thus improved by 50% compared with the undoped double layer film (Fig. 2). With $t_{nom}=2\times215$ nm YBCO and Ag deposited between the layers, a $J_c$(77 K) value of $5.6\times10^6$ A/cm$^2$ was achieved (Fig. 2). This value is five times the value for the Ag doped single layer 430 nm film, and is an order magnitude larger than the value for the undoped single layer 400 nm film (Fig. 2). In terms of the microbridge device introduced above this means that a maximum current of almost 25 mA can be applied without affecting the superconductivity of the device. We have thus compensated for the large decrease in $J_c$(77 K) for films with $t_{nom}>300$ nm.

In a similar experiment, an Ag doped double layer 730 nm film was grown consisting of a first layer of 300 nm Ag doped film and a second layer of 430 nm film. The annealing was done using the prescriptions outlined above. The film was hard but had extended surface structures (Fig. 10). However, $J_c$(77 K) was quite low with a value of $7.6\times10^5$ A/cm$^2$ (Fig. 8). From Fig. 8 it seems there is a small kink in the $J_c-T$ curve at 79 K indicating the presence of 1–2–4 inclusions. These inclusions are probably present only in the first 300 nm layer. This experiment thus shows that the multilayer films should indeed be fabricated from films with $t_{nom}<300$ nm.

## V. CONCLUSIONS

In summary, we have shown that the current carrying capacities of post annealed YBCO thin films can be improved by doping with Ag prior to the annealing. This improvement is primarily due to a better epitaxial structure of the YBCO film in the presence of Ag during growth. Also, we have shown that the value of $J_c$(77 K) is critically dependent on the presence of a large number of 1–2–4 inclusions in the 1–2–3 matrix irrespective of the doping characteristics (undoped/Ag doped) and the growth method (single layer/multilayer). The 1–2–4 inclusions become superconducting around 80 K and make a significant contribution to the total supercurrent below that temperature. The formation of 1–2–4 inclusions during the annealing sequence is intimately linked to the annealing temperature ($T_{ann}$), gas pressure ($p(O_2)$) and time ($t_{ann}$).


[1] S.-W. Chan, B. G. Bagley, L. H. Greene, M. Giroud, W. L. Feldmann, K. R. Jenkin, and B. J. Wilkins, Appl. Phys. Lett. **53**, 1443 (1988).
[2] X. K. Wang, K. C. Sheng, S. J. Lee, Y. H. Shen, S. N. Song, D. X. Li, R. P. H. Chang, and J. B. Ketterson, Appl. Phys. Lett. **54**, 1573 (1989).
[3] M. P. Siegal, J. M. Phillips, R. B. van Dover, T. H. Tiefel, and J. H. Marshall, J. Appl. Phys. **68**, 6353 (1990).
[4] A. Mogro-Campero, L. G. Turner, A. M. Kadin, and D. S. Mallory, Appl. Phys. Lett. **60**, 3310 (1992).
[5] M. P. Siegal, S. Y. Hou, J. M. Phillips, T. H. Tiefel, and J. H. Marshall, J. Mater. Res. **7**, 2658 (1992).
[6] A. Mogro-Campero, L. G. Turner, A. M. Kadin, and D. S. Mallory, J. Appl. Phys. **73**, 5295 (1993).
[7] S. Y. Hou, J. M. Phillips, D. J. Werder, T. H. Tiefel, J. H. Marshall, and M. P. Siegal, J. Mater. Res. **9**, 1936 (1994).
[8] R. W. Simon, C. E. Platt, A. E. Lee, G. S. Lee, K. P. Daly, M. S. Wire, J. A. Luine, and M. Urbanik, Appl. Phys. Lett. **53**, 2677 (1988).
[9] Unpublished results.
[10] M. Z. Cieplak, G. Xiao, C. L. Chien, J. K. Stalick, and J. J. Rhyne, Appl. Phys. Lett. **57**, 934 (1990).
[11] R. K. Singh, D. Bhattacharya, P. Tiwari, J. Narayan, and C. B. Lee, Appl. Phys. Lett. **60**, 255 (1992).
[12] T. Kumagai, T. Manabe, W. Kondo, S. Mizuta, and K. Arai, Appl. Phys. Lett. **61**, 988 (1992).
[13] R. Pinto, N. Goyal, S. P. Pai, P. R. Apte, L. C. Gupta, and R. Vijayaraghavan, J. Appl. Phys. **73**, 5105 (1993).
[14] S. S. Ata-Allah, Y. Xu, and C. Heiden, Physica C **221**, 39 (1993).
[15] A. K. Pradhan, B. K. Roul, V. V. Rao, and V. R. Kalvey, Cryogenics **33**, 910 (1993).
[16] C. N. van Huong, M. Nicolas, A. Dubon, and C. Hinnen, J. Mater. Sci. **28**, 6418 (1993).
[17] M. J. Day, S. D. Sutton, F. Wellhofer, and J. S. Abell, Supercond. Sci. Technol. **6**, 96 (1993).
[18] D. Veretnik and S. Reich, Physica C **223**, 227 (1994).
[19] D. Kumar, M. Sharon, P. R. Apte, R. Pinto, S. P. Pai, S. C. Purandare, C. P. D'Souza, L. C. Gupta, and R. Vijayaraghavan, J. Appl. Phys. **76**, 1349 (1994).
[20] P. R. Apte, R. Pinto, A. G. Chourey, and S. P. Pai, J. Appl. Phys. **75**, 4258 (1994).
[21] R. Pinto, P. R. Apte, M. S. Hedge, and D. Kumar, J. Appl. Phys. **77**, 4116 (1995).
[22] A. Sen and H. S. Maiti, Physica C **229**, 188 (1994).
[23] T. Clausen, M. Ejrnaes, M. Olesen, K. Hilger, J. L. Skov, P. Bodin, A. Kühle, and I. Chorkendorff, Appl. Phys. Lett. **65**, 2350 (1994).
[24] E. Yanmaz, I. H. Mutlu, T. Kucukomeroglu, and M. Altunbas, Supercond. Sci. Technol. **7**, 903 (1994).
[25] A. Lanckbeen, P. H. Duvigneaud, P. Diko, M. Mehbod, G. Naessen, and R. Deltour, J. Mater. Sci. **29**, 5441 (1994).
[26] P. Selvam, Appl. Phys. Lett. **67**, 3650 (1995).
[27] P. C. McIntyre and M. J. Cima, J. Mater. Res. **9**, 2778 (1994).
[28] A. F. Marshall, K. Char, R. W. Barton, A. Kapitulnik, and S. S. Laderman, J. Mater. Res. **5**, 2049 (1990).
[29] B. M. Clemens, C. W. Nieh, J. A. Kittl, W. L. Johnson, J. Y. Josefowicz, and A. T. Hunter, Appl. Phys. Lett. **53**, 1871 (1988).
[30] G. F. Voronin and S. A. Degterov, Physica C **176**, 387 (1991).